

The polarization sensitivity of GRETINA

C. Morse^{a,b,*}, H.L. Crawford^a, A.O. Macchiavelli^a, A. Wiens^a, M. Albers^c, A.D. Ayangeakaa^{h,i}, P.C. Bender^g,
C.M. Campbell^a, M.P. Carpenter^c, P. Chowdhury^d, R.M. Clark^a, M. Cromaz^a, H.M. David^c, P. Fallon^a,
R.V.F. Janssens^{h,i}, T. Lauritsen^c, I.-Y. Lee^a, C.J. Lister^d, D. Miller^g, V.S. Prasher^d, S.L. Tabor^f, D. Weisshaar^e,
S. Zhu^{c,b,1}

^a*Nuclear Science Division, Lawrence Berkeley National Laboratory, Berkeley, CA 94720, USA*

^b*National Nuclear Data Center, Brookhaven National Laboratory, Upton, New York 11973, USA*

^c*Physics Division, Argonne National Laboratory, Lemont, IL 60439, USA*

^d*Department of Physics and Applied Physics, University of Massachusetts Lowell, Lowell, MA 01854, USA*

^e*National Superconducting Cyclotron Laboratory, Michigan State University, East Lansing, MI 48824, USA*

^f*Department of Physics, Florida State University, Tallahassee, FL 32306, USA*

^g*TRIUMF, Vancouver, British Columbia, Canada V6T 2A3*

^h*Department of Physics and Astronomy, University of North Carolina at Chapel Hill, Chapel Hill, NC 27599, USA*

ⁱ*Triangle Universities Nuclear Laboratory, Duke University, Durham, NC 27708, USA*

Abstract

Compton polarimeters have played an important role in the study of nuclear structure physics, but have often been limited in their applications because of relatively low γ -ray detection efficiency. With the advent of γ -ray tracking detector arrays, which feature nearly 4π solid angle coverage and the ability to identify the location of Compton-scattering events to within a few millimeters, this limitation can be overcome. Here we present a characterization of the performance of the Gamma Ray Energy Tracking In-beam Nuclear Array (GRETINA) as a Compton polarimeter using the $^{24}\text{Mg}(p, p')$ reaction at 2.45 MeV proton energy. We also discuss a new capability added to the simulation package UCGretina to simulate the emission of polarized photons, and compare it to the measured data. Finally, we use these simulations to predict the performance of the Gamma Ray Energy Tracking Array (GRETA).

Keywords: Polarization, tracking detectors

1. Introduction

Characterization of the spins and parities of nuclear states is fundamental to nuclear structure physics. These important quantum numbers can often be inferred in a number of ways; examples include the selectivity of the nuclear reaction used, decay selection rules, systematics, and/or comparison with theoretical calculations. However, a direct measurement is clearly preferable. The angular distribution of γ -rays emitted from excited states can be used for spin assignment, but as electric and magnetic transitions of the same multipolarity have the same angular dependence, such distributions cannot provide insight into parity. In contrast, when γ rays undergo Compton scattering, they will preferentially scatter in directions perpendicular to the electric field vector of the incoming photon. This sensitivity provides a means to differentiate between electric and magnetic transitions, and forms the basic operating principle for Compton polarimeters.

The first Compton polarimeter was described in 1950, and used a pair of scintillator detectors to achieve polar-

ization sensitivity [1]. Since that time, Compton polarimeters have evolved to use many different configurations and technologies [2–10]. The newest generation of γ -ray spectrometers [11], including the Gamma-Ray Energy Tracking In-beam Nuclear Array (GRETINA) [12], its successor the Gamma-Ray Energy Tracking Array (GRETA) [13], and the Advanced GAMMA Tracking Array (AGATA) [14], are inherently powerful Compton polarimeters. Generally, a Compton polarimeter provides a measurement of the azimuthal and polar scattering angle between the first and the second locations where a photon interacts with a detector. Historically, this has been accomplished with dedicated experimental setups using multiple detectors in specific geometries which offered high sensitivity, but very limited efficiency. In contrast, γ -ray tracking arrays can determine the Compton scattering angles throughout their active volumes. These arrays benefit from their fine effective granularity, which arises from the inherent electronic segmentation and the ability to locate γ -ray interaction points with sub-segment resolution through pulse-shape analysis, or signal decomposition. With full knowledge of the energies and angles between each interaction, tracking detectors are uniquely suited as Compton polarimeters, combining high sensitivity with high efficiency for γ -ray

*Corresponding author

Email address: cmorse@bnl.gov (C. Morse)

¹Deceased

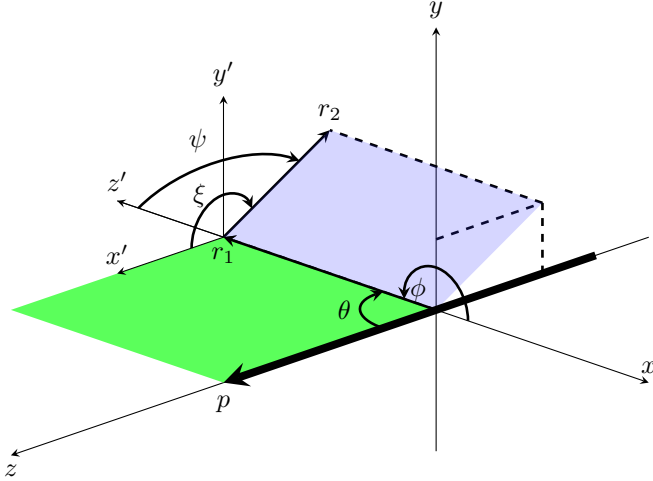


Figure 1: An illustration of the relevant angles involved in an experiment measuring linear polarization. The coordinates $\{\theta, \phi\}$ are the polar and azimuthal angles of the vector \vec{r}_1 , along which a photon is emitted from an excited nucleus at the origin. The primed coordinate system is determined by the emission direction of the photon (z'), with x' lying in the reaction plane and y' defined by the right hand rule. The angles $\{\psi, \xi\}$ are the polar and azimuthal angles of the vector \vec{r}_2 , along which the photon Compton scatters, expressed in the primed coordinate system. See text for details.

detection, as has been already demonstrated [15–17].

In this work, we characterize GRETINA as a Compton polarimeter. The next section presents background information relevant to GRETINA and the concepts of Compton scattering and linear polarization of γ -rays. This is followed by discussion of a dedicated experiment performed to evaluate the sensitivity of GRETINA as a Compton polarimeter, including details of the measurement and analysis of the data. Finally, the GRETINA performance is benchmarked against Monte Carlo simulations, and extrapolated to predict the performance of the complete 4π GRETA spectrometer.

2. Background

2.1. Definitions and terminology

A nuclear state may be characterized by an angular momentum I (colloquially called “spin”) and its projection M along a quantization axis (where $-I \leq M \leq I$). When an excited state I_i is created, the magnetic substates M_i will be populated with probability $P(M_i)$. If the population of the magnetic substates is uneven (i.e. $P(M_i) \neq \frac{1}{2I_i+1}$ for all M_i), the state is said to be *oriented*. There are two types of orientation: if $P(M_i) = P(-M_i)$ for all M_i , then the state is said to be *aligned*; otherwise, the state is said to be *polarized*. The (p, p') reaction used in this work can only create aligned nuclear states, as the proton beam establishes an axis of symmetry but not a preferred direction [18].

Characterization of a detector as a polarimeter involves discussion of several distributions. Figure 1 illustrates the

relevant angles discussed in this study. A proton beam excites target nuclei at the origin, with the bold arrow indicating the beam direction. The excited nucleus emits a photon that undergoes Compton scattering at the point r_1 , and interacts again at the point r_2 . The proton beam defines the z -axis of the laboratory frame, while the coordinates $\{\theta, \phi\}$ represent the emission angle of the photon in this frame. The beam axis and the vector r_1 define the *reaction plane*, shaded green in Fig. 1 (for references to color, see the online version of this manuscript). The direction of the scattered photon can be expressed by the angles $\{\psi, \xi\}$ in the coordinate system $\{x', y', z'\}$, where z' is in the direction of the photon emission, x' lies in the reaction plane, and y' is defined by the right-hand rule. The vectors \vec{r}_1 and \vec{r}_2 define the *scattering plane*, shaded blue in Fig. 1.

The polar angular distribution of γ rays emitted by an excited state is characteristic of the multipolarity of the photon. Because of the selection rules for electromagnetic decay, this distribution conveys information about the initial and final-state spins as well as the initial magnetic substate population. The distribution for an aligned initial state has been described extensively in the literature [6, 7, 18–20]. In practice, the functional form of the angular distribution that is fit to experimental data is described by a Legendre polynomial series:

$$W(\theta) = \sum_{\substack{k=0, \\ \text{even}}}^{2I_i} a_k P_k(\cos \theta), \quad (1)$$

where the coefficients a_k carry the information on the population of the magnetic substates $P(M_i)$ ($a_0 = 1$). The requirement that k be even is specific to the case of an aligned initial state. The degree to which the emitted γ rays are polarized can be calculated from the a_k coefficients. For the case of a pure dipole or quadrupole transition [6],

$$P(\theta) = \Pi \frac{\frac{1}{2}a_2 P_2^{(2)}(\cos \theta) - \frac{1}{12}a_4 P_4^{(2)}(\cos \theta)}{1 + a_2 P_2(\cos \theta) + a_4 P_4(\cos \theta)}, \quad (2)$$

where $P_k^m(\cos \theta)$ are associated Legendre polynomials, Π is the parity of the photon, and the polarization is restricted to the range $-1 \leq P \leq 1$. The degree of polarization is often quoted at $\theta = 90^\circ$, since $P_k(\cos 90^\circ)$ and $P_k^m(\cos 90^\circ)$ can be expressed as rational numbers:

$$P(\theta = 90^\circ) = \Pi \frac{\frac{3}{2}a_2 + \frac{5}{8}a_4}{1 - \frac{1}{2}a_2 + \frac{3}{8}a_4}. \quad (3)$$

The parity Π in Eqs. 2 and 3 cannot be determined from the a_2 and a_4 coefficients alone. A Compton polarimeter can resolve this ambiguity by exploiting the dependence of the Compton-scattering cross section on the linear polarization of the photon. This sensitivity is expressed through the Klein-Nishina formula, which for a linearly polarized

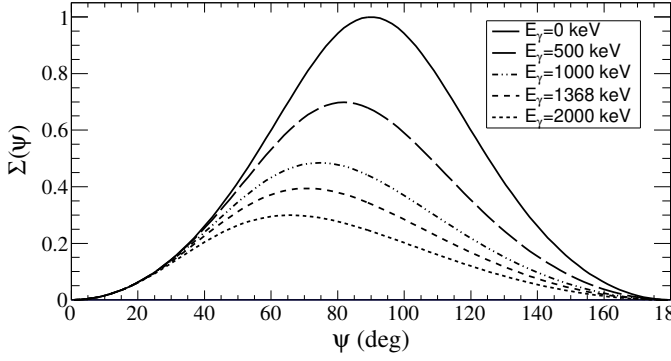


Figure 2: The analyzing power $\Sigma(\psi)$, plotted for several different γ -ray energies.

γ ray takes the form [21]

$$\frac{d\sigma}{d\Omega}(\psi, \chi) = \frac{1}{2} r_e^2 \left(\frac{E'_\gamma}{E_\gamma} \right)^2 \left[\frac{E'_\gamma}{E_\gamma} + \frac{E_\gamma}{E'_\gamma} - 2 \sin^2 \psi \cos^2 \chi \right], \quad (4)$$

where r_e is the classical electron radius, ψ is the Compton scattering angle in Fig. 1, χ is the angle between the electric field vector of the incident photon and the Compton scattering plane, and E_γ and E'_γ are the incident and scattered photon energy, respectively. The $\cos^2 \chi$ dependence in the Compton-scattering cross section indicates that scattering perpendicular to the electric field vector is preferred. However, it is more convenient to transform Eq. 4 into an angular distribution in terms of the angle ξ in Fig. 1. This transformation is detailed in Ref. [16], with the result

$$W_c(\theta, \psi, \xi) = W(\theta) \frac{d\sigma}{d\Omega}(\psi) \left[1 - \frac{1}{2} \Sigma(\psi) P(\theta) \cos 2\xi \right] \quad (5)$$

where $\Sigma(\psi)$ is known as the *analyzing power*, and the lack of ξ dependence in $\frac{d\sigma}{d\Omega}(\psi)$ denotes the cross section for unpolarized photons. The sign of the $\cos 2\xi$ distribution determines the parity Π in Eq. 2. The analyzing power Σ is given by

$$\Sigma(\psi) = \frac{\sin^2 \psi}{\frac{E'_\gamma}{E_\gamma} + \frac{E_\gamma}{E'_\gamma} - \sin^2 \psi} \quad (6)$$

and represents the theoretical limit for the sensitivity of a Compton polarimeter. Fig. 2 depicts the analyzing power as a function of ψ for several different γ -ray energies.

When performing a linear polarization measurement, practically one chooses range of θ and ψ over which to measure and then inspects the distribution of azimuthal Compton-scattering angles ξ . Thus, Eq. 5 becomes

$$W_c(\xi) = b(1 - A_0 \cos 2\xi), \quad (7)$$

where A_0 is the asymmetry in the ξ distribution which serves as the key observable in Compton polarimetry. Comparing Eq. 7 with Eq. 5, clearly A_0 depends on the average value of the polarization and the analyzing power

for the data under consideration. However, for a given polarization, a real polarimeter may measure an asymmetry smaller than that expected from Eq. 6. Therefore, the *polarization sensitivity* Q can be defined, which serves as an effective analyzing power for a given polarimeter such that

$$A_0 = \frac{1}{2} Q \bar{P}, \quad (8)$$

where \bar{P} is the average value of the polarization over the chosen range of θ . This definition agrees with the one adopted for AGATA in Ref. [16]. Often the relationship between the analyzing power and the polarization sensitivity is expressed simply as an energy-dependent scaling between Q and Σ for an idealized polarimeter composed of point-like detectors (e.g. Refs. [22, 23]). Characterizing Q for a polarimeter thus allows an experimenter to predict what asymmetry may be measured for a given γ -ray energy and polarization.

Maximizing Q is an important design element for a Compton polarimeter. However, it is also important to consider the detection efficiency of the system. For example, one might choose to place detectors only where the analyzing power is expected to be largest, but doing so may require a longer measurement to reach a given precision. In order to gauge whether a loss of statistics is justified by a corresponding gain in Q , a figure of merit was proposed which takes the form [24]

$$F = Q^2 \varepsilon, \quad (9)$$

where ε is the efficiency of the polarimeter to register an event. For a tracking detector, the relevant quantity is the efficiency to detect a Compton-scattering event, since it is impossible to define a scattering plane without at least two interaction points.

2.2. GRETINA Signal Decomposition and Position Resolution

GRETINA is built of 36-fold segmented, hexagonally shaped and tapered high-purity Germanium (HPGe) detector crystals [12]. Two slightly different irregular asymmetric crystal shapes are used and housed together in Quad modules of four individually encapsulated detectors, including two of each shape. The final design of GRETINA is composed of 12 such Quad modules; at the time of the experiment described in this manuscript, the array included only six Quad modules.

Each individually encapsulated detector crystal operates independently to record data. When a γ ray interacts with a crystal volume, triggering a full-volume signal above threshold, the core contact and all 36 segment-electrode signals are digitized simultaneously. To locate interaction points in the crystal, the experimental signals are fitted against linear combinations of signals derived from a detector simulation. As a result of this fit, multiple interactions within the crystal volume can be located and their relative energies determined. This process is referred to

147 as signal decomposition, and results in a set of interaction
 148 point coordinates which can then be interpreted as Compton
 149 scattering or photoelectric absorption of γ rays in the
 150 crystal volumes.

The precision with which the decomposition process determines interaction-point positions has been the subject of previous investigations. A collimated ^{137}Cs source was used to determine the position resolution of GRETINA at 662 keV [12]. The results of this study showed that the interaction-point positions could be determined with a precision $\sigma \approx 2$ mm. In addition, a radioactive beam experiment examined the position resolution that could be achieved under more typical operating conditions [25]. A position resolution of $\sigma = 1.2$ mm at 1779 keV was inferred from this analysis. Similar investigations have been carried out for AGATA [26], finding that the energy dependence of the position resolution could be described by the function

$$\sigma(e) = a + b/\sqrt{e}, \quad (10)$$

151 where e is the energy deposited at a given interaction
 152 point. Compton polarimetry is critically dependent on
 153 the determination of the scattering plane defined by the
 154 coordinates of the first two interaction-point positions for
 155 a scattered γ ray, so these prior investigations are an im-
 156 portant guide for the present work.

157 3. Experiment

158 In order to characterize the performance of GRETINA¹⁸⁶
 159 as a Compton polarimeter, the $^{24}\text{Mg}(p,p')$ reaction at¹⁸⁷
 160 2.45 MeV proton energy was chosen as a source of lin-¹⁸⁸
 161 early polarized γ rays. This reaction has been studied¹⁸⁹
 162 many times in the past (e.g. [3, 4, 7, 23, 27]), and has¹⁹⁰
 163 been shown to produce photons which are nearly 100%¹⁹¹
 164 polarized at $\theta = 90^\circ$. The high degree of polarization¹⁹²
 165 can be understood by considering the maximum angular¹⁹³
 166 momentum $\vec{L} = \vec{r} \times \vec{p}$ which can be transferred to the nu-¹⁹⁴
 167 cleus. This quantity can be estimated based on the contact¹⁹⁵
 168 distance $r = 1.2(A_p^{1/3} + A_{^{24}\text{Mg}}^{1/3})$ fm, which for the stated¹⁹⁶
 169 beam energy gives a maximum angular momentum trans-¹⁹⁷
 170 fer of $L \approx 1.6\hbar$. Thus, the population of the $M = \pm 2$ ¹⁹⁸
 171 magnetic substates is strongly suppressed in this reaction,¹⁹⁹
 172 resulting in a highly aligned excited state. In addition, the²⁰⁰
 173 only excited state that can be populated at this beam en-²⁰¹
 174 ergy is the 2^+ state at 1368.7 keV [28]. The next excited²⁰²
 175 state in ^{24}Mg is a 4^+ state at 4122.9 keV [28], which is²⁰³
 176 clearly not accessible at the present beam energy. There-²⁰⁴
 177 fore, any decays from the 2^+ state must be the result of²⁰⁵
 178 direct population and not feeding from above.²⁰⁷

179 The experiment was performed at Argonne National²⁰⁸
 180 Laboratory. A proton beam was accelerated to 2.45 MeV²⁰⁹
 181 by the Argonne Tandem Linear Accelerator System (AT-²¹⁰
 182 LAS) and delivered to the experimental area. The beam²¹¹
 183 was impinged on a 3.3-mg/cm² natural magnesium tar-²¹²
 184 get, and photons emitted from the deexcitation of magne-²¹³
 185 sium nuclei were detected with GRETINA. For this exper-²¹⁴

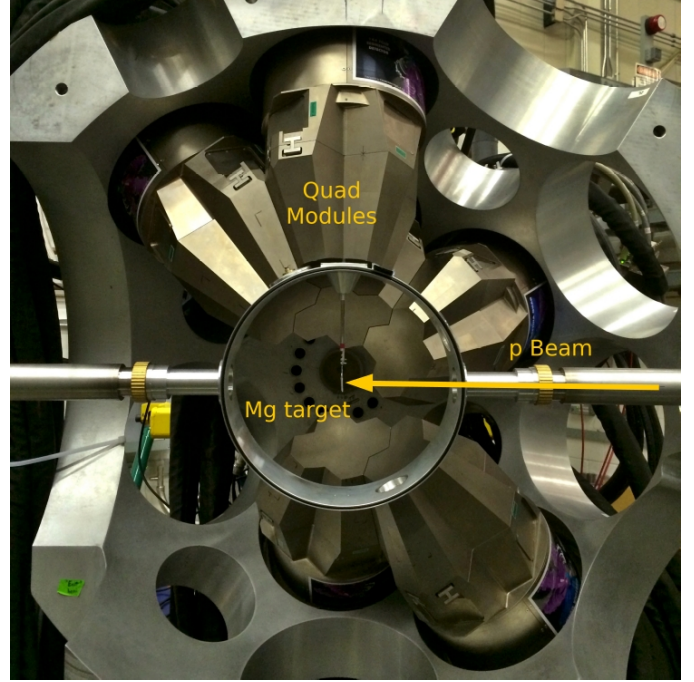


Figure 3: A photograph of the experimental setup, showing the arrangement of the six GRETINA Quad modules used in this work. The target is also visible in the center of the figure; from this perspective, the beam would impinge on the target from the right-hand side of the figure.

186 inment, the six modules were arranged in one hemisphere
 187 in order to maximize the detection efficiency for Compton-
 188 scattered photons, as shown in Fig. 3. Three detector mod-
 189 ules were placed at polar angles of 90° , where the degree
 190 of linear polarization is expected to be largest. Two of the
 191 remaining Quads were placed at backward angles and one
 192 at forward angles. In total, the array covered polar angles
 193 spanning from 40 - 140° .

Data were taken for the (p,p') reaction for approxi-
 194 mately ten hours at a typical beam current of 10 nA.
 195 Data were also taken with a ^{60}Co source placed at the
 196 target position of GRETINA to provide a source of un-
 197 polarized γ rays. The γ -ray tracking algorithm developed
 198 for GRETINA data [29] was applied to both the source
 199 and the in-beam data, in order to reconstruct those events
 200 for which full-energy deposition occurred through multi-
 201 ple interactions between the photons and the array. The
 202 clustering angle used in the tracking algorithm was set to
 203 20° , in agreement with the recommendation in Ref. [29].
 204 Increasing the clustering angle beyond 20° did not yield
 205 significantly greater statistics. The resulting γ -ray spectra
 206 are shown in Fig. 4, with panel (a) showing the $^{24}\text{Mg}(p,p')$
 207 data and panel (b) showing the ^{60}Co data. The tracking
 208 algorithm assigns a figure of merit to tracked γ -rays (dis-
 209 tinct from the figure of merit discussed in Sect. 2.1), with
 210 lower values corresponding to better agreement with the
 211 characteristics expected for a Compton-scattering event.
 212 At this stage of the analysis, no restriction was placed on
 213 the tracking figure of merit. The effect of selecting only

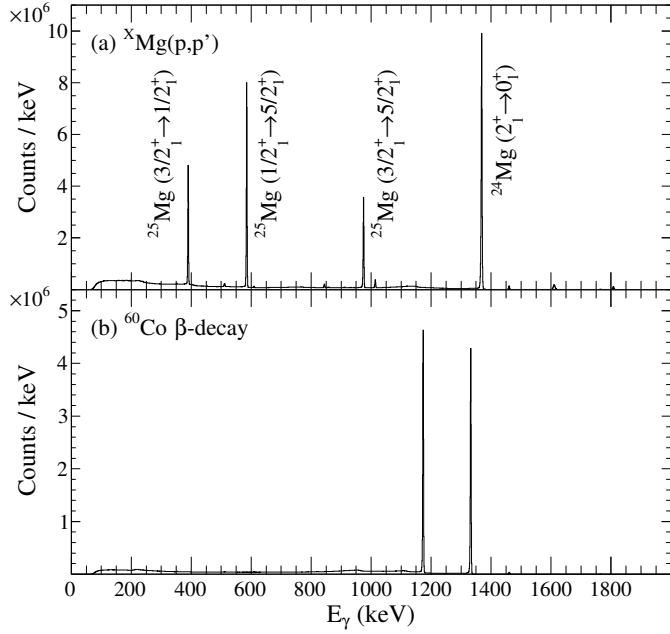


Figure 4: Tracked γ -ray spectra from GREYINA for (a) 2.45 MeV protons incident on a natural magnesium target, labeled according to transition and isotope, and (b) a ^{60}Co source.

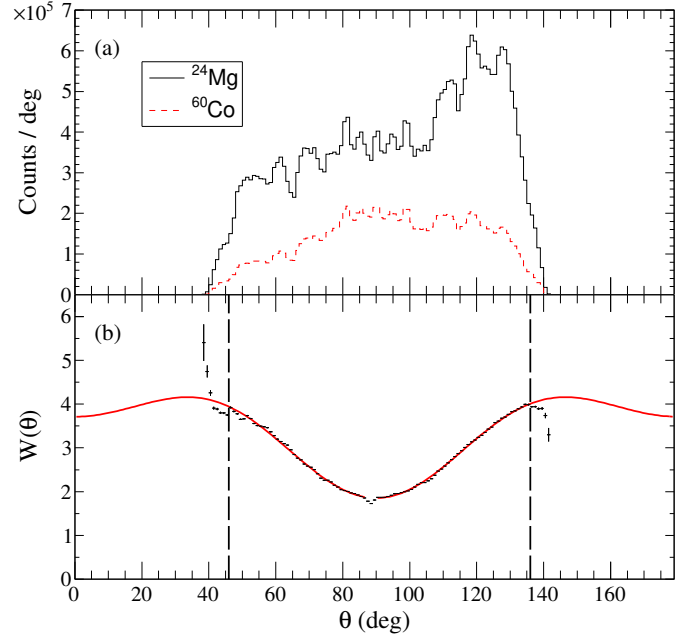


Figure 5: (a) Polar angular distribution of the γ rays detected for the $2_1^+ \rightarrow 0_1^+$ transition populated in $^{24}\text{Mg}(p, p')$ (solid line) and β^- decay of ^{60}Co (dashed line). (b) The ratio of the ^{24}Mg distribution and ^{60}Co distribution shown in (a).

events with a figure of merit below some threshold is discussed at the end of this section.

The distribution of events detected at a given polar angle for the in-beam and source data were generated by selecting those events which fell within an energy range corresponding to the $2_1^+ \rightarrow 0_1^+$ transitions in ^{24}Mg and ^{60}Ni (the β^- -decay daughter of ^{60}Co), located respectively at 1368 keV and 1332 keV, and plotting the angle at which the first interaction point was detected relative to the beam direction. Background events were taken into account by subtracting angular distributions generated from regions on both the high-energy and low-energy sides of the peaks with half the width of the regions of interest. The resulting angular distributions are shown in Fig. 5(a). Since the source data is uncorrelated with the beam direction, the features of the dashed line arise solely from the geometry of the GREYINA array. The ratio of the in-beam to the source distribution, shown in Fig. 5(b) with error bars corresponding to the statistical uncertainties, removes these geometrical effects (the small difference in detection efficiency between $E_\gamma = 1332$ keV and $E_\gamma = 1368$ keV is neglected).

The angular distribution exhibits several deviations from the expected shape, particularly at the most forward and backward angles. In addition, there is a small deficit in counts at 87° . One possible explanation for these features is a small offset of the source and/or beamspot from the center of the GREYINA array, or that the beam direction is rotated slightly relative to the z-axis of GREYINA. An attempt was made to determine whether there was any such offset/rotation by including these in the fitting procedure, but meaningful improvement could not be found.

Another explanation for the irregularities could be problems with the signal decomposition process. Decomposition errors are known to occur which cause interaction points to cluster around the central contact and at the segment boundaries at the edges of the crystals, and typically occur more frequently for lower-energy interactions. Several central contacts happen to coincide at about 87° , so this effect seems likely to be the source of the feature at this angle. Similarly, the decomposition errors located at the crystal boundaries may result in the decrease in the angular distribution at backward angles, where there is relatively less germanium material present to wash out such artifacts. This effect is likely masked at forward angles by a separate issue which was discovered during the analysis. The sole crystal which was located at the most forward angles failed to assign interactions points properly to a significant fraction of the segments, which is likely why the angular distribution fluctuates in this region. Regardless, these issues do not compromise the overall performance of GREYINA as a polarimeter, as the angular distribution is still clearly that of a quadrupole transition.

The solid line in Fig. 5(b) is the result of a fit with Eq. 1, with a scaling factor to account for the different number of counts in the in-beam data and source data. The vertical dashed lines denote the range over which the data was fit with this function, which was chosen to maximize the angular range included in the fit while excluding the extremes which obviously do not follow a Legendre polynomial distribution. The gap in the solid line denotes bins

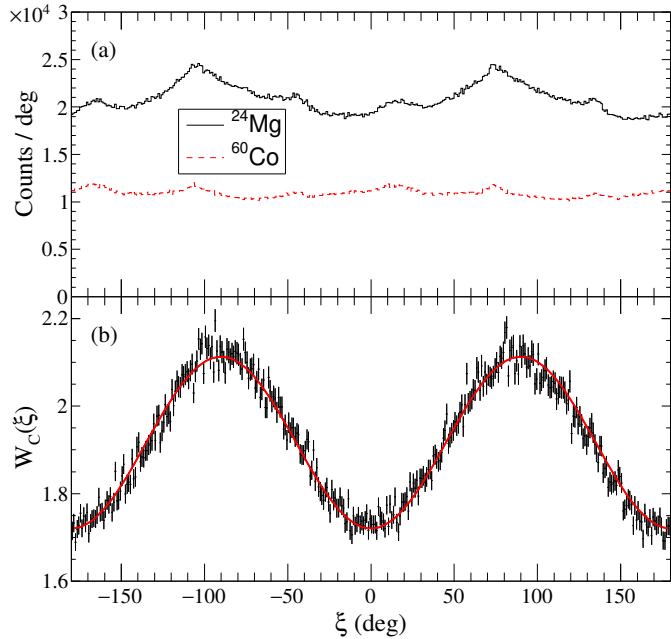


Figure 6: (a) Azimuthal angular distribution of Compton scattered photons for the $2_1^+ \rightarrow 0_1^+$ transition populated in $^{24}\text{Mg}(p, p')$ (solid line) and ^{60}Co β^- decay (dashed line). The polar angle of the first interaction point is restricted to $80^\circ \leq \theta \leq 100^\circ$. (b) The ratio of the ^{24}Mg distribution and ^{60}Co distribution shown in (a).

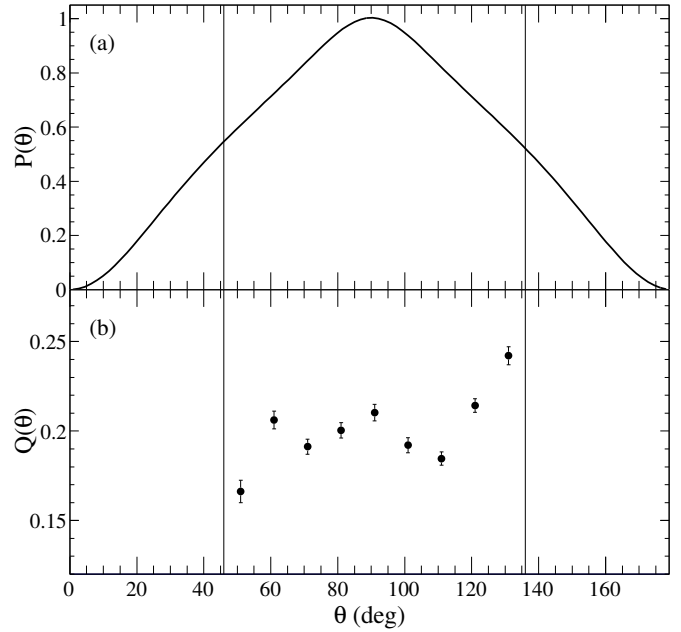


Figure 7: (a) Polarization as a function of θ as given by Eq. 2, with $a_2 = 0.545$ and $a_4 = -0.351$. (b) Q calculated for events in 10° slices of θ . There is significant scatter in the data points, but aside from the edges of the array the values are roughly constant.

which were not included in the fit, corresponding to the region where several central contacts are located. The expansion coefficients resulting from the fit to the angular distribution are $a_2 = 0.545(5)$ and $a_4 = -0.351(5)$. Using these values in Eq. 3 gives a polarization for photons emitted at 90° of $P(\theta = 90^\circ) = 1.00(2)$.

The distribution of azimuthal Compton scattering angles was constructed using tracked events which have at least two interaction points. The same energy ranges were used to construct both the polar angular distribution and the azimuthal distribution. Since the degree of linear polarization is expected to be highest near $\theta = 90^\circ$, the polar angle of the first interaction point was restricted to lie in the range $80^\circ \leq \theta \leq 100^\circ$. The resulting distributions are shown in Fig. 6(a), with the $^{24}\text{Mg}(p, p')$ data shown by the solid line and the ^{60}Co β -decay data by the dashed line. The features in the source distribution, which should in principle be flat, arise from the geometry of the GRETINA array and can also be seen in the in-beam distribution. The ratio of these two distributions is shown in Fig. 6(b), with statistical error bars included, and clearly exhibits the expected sinusoidal behavior based on Eq. 7. The solid line is a fit to the data with Eq. 7, resulting in an asymmetry $A_0 = 0.1024(9)$.

While the asymmetry demonstrated in Fig. 6 is clear evidence that GRETINA can act as a Compton polarimeter, we now calculate Q and the figure of merit defined in Sect. 2.1 in order to compare the performance of the array with other polarimeters. Equation 8 can be inverted to find that $Q = 2A_0/\bar{P}$, where A_0 is the measured asym-

metry in the ξ distribution. Fig. 7(a) shows the function $P(\theta)$ determined from Eq. 2, with a_2 and a_4 coefficients taken from the fit in Fig. 5(b). The average polarization, weighted according to the solid angle covered by the array, is $\bar{P} = 0.824(8)$ and results in $Q = 0.196(2)$. Since the polarization sensitivity should be not be a function of θ , Q was also determined in 10° -wide bins over the range within the vertical lines in the figure, with the results plotted in Fig. 7(b). While there is considerable scatter among the data points, they remain reasonably constant at a value of about 0.2 for most of the angular range considered. The notable exceptions are at the far forward and backward angles, and may be related to the deviations at the extremes of the polar angular distribution which were discussed earlier.

Determining the figure of merit defined by Eq. 9 requires that the detection efficiency be known. The absolute singles efficiency of GRETINA was reported in Ref. [25], albeit in a configuration with eight Quad modules instead of six. Therefore, the reported efficiency was scaled by a factor of 0.75 in order to account for the different number of GRETINA modules, and in order to be conservative the reported uncertainties were doubled. This resulted in an untracked efficiency for this experiment of $\varepsilon(1368 \text{ keV}) = 3.71(7)\%$. Multiplying by the ratio of the counts in the tracked and untracked photopeaks gives the tracked efficiency (excluding events with only one interaction point). The resulting efficiency is $5.3(1)\%$ for the geometry used in the present experiment, which gives a figure of merit $F = 2.04(6) \times 10^{-3}$. Table 1 lists the performance

Table 1: A comparison of the performance of GRETINA as a Compton polarimeter with several other polarimeters which have been characterized in the literature. GRETINA is competitive on the basis of its polarization sensitivity Q , although there are clearly more sensitive detectors. However, its figure of merit is orders of magnitude better than the other entries in the table due to its much higher detection efficiency, which demonstrates the power of the array as a polarimeter. A prediction of the performance of GRETA is given in Sect. 4.4.

Detector or author	Q (1368 keV)	Figure of merit
GRETINA	0.196	2.0×10^{-3}
DAGATA [16]	0.192 ^a	-
POLALI [22]	0.30	1.8×10^{-6}
MINIPOLA [22]	0.05	3.0×10^{-8}
GAMMASPHERE [27]	0.043	1.7×10^{-6}
Schlitt[7]	0.15	1.0×10^{-6}
Butler[4]	0.274	-
Litherland[3]	0.066 ^b	-
Litherland[3]	0.072 ^b	-
Jones[23]	0.121	-

^a Measured at 1332 keV with ^{60}Co source

^b Corrected by factor of 2 to use a consistent definition of Q

of GRETINA in the configuration used for this experiment as well as several other detectors which have been characterized as polarimeters. The value of Q for GRETINA is competitive with other detectors, but in terms of its figure of merit it is superior by several orders of magnitude. This is due to the greatly increased efficiency. As an example, one can contrast the figure of merit for GRETINA with that of the polarimeter described by Schlitt *et al.* [7]. The two systems differ in Q by about 40%, while the figures of merit differ by a factor of 2000. This is understood almost entirely as a result of the efficiency, where the detectors of Ref. [7] are individually approximately a factor of 3 less efficient than a single GRETINA crystal, due largely to the distance from the target. This gives rise to an order of magnitude when one realizes the requirement of a coincidence measurement, which is compounded by another order of magnitude as there were 24 crystals used in the GRETINA measurement. Given the importance of the efficiency in the definition of the figure of merit discussed here, one realizes that the performance of GRETA should be much better even than GRETINA, as will be discussed in Sect. 4.4. It is also worth noting that the analyzing power (i.e. Q) of AGATA has been measured at other energies, reaching values of nearly 0.5 for $E_\gamma \approx 500$ keV [15].

The analysis above has treated the entire data set collected with GRETINA. It is possible to be more selective in the analysis in order to enhance the polarization sensitivity, but at the price of lower efficiency. Table 2 explores the effect that a few such cuts have on both Q and the

Table 2: The effect that placing various cuts on the data has on the polarization sensitivity Q and the figure of merit F . In general, any gain in Q from a given cut is at best offset by the loss in efficiency when calculating the figure of merit. Note that F_t indicates the figure of merit associated with the tracking algorithm, not Eq. 9.

Cut	$Q(1368 \text{ keV})$	$F(1368 \text{ keV})$
None	0.196(2)	$2.04(6) \times 10^{-3}$
$F_t \leq 0.6$	0.210(2)	$2.00(6) \times 10^{-3}$
$F_t \leq 0.1$	0.314(5)	$5.1(2) \times 10^{-4}$
$60^\circ \leq \psi \leq 80^\circ$	0.267(3)	$8.0(3) \times 10^{-4}$

figure of merit F . Restricting the tracking figure of merit (denoted F_t in the table) to values of 0.6 or less, consistent with the recommendation in Ref. [29], should exclude events which do not agree very well with the characteristics expected for Compton scattering. In fact, there is a small increase in the polarization sensitivity when this cut is applied, but there is also a small decrease in the polarization figure of merit due to lost efficiency. Placing a more stringent requirement that the tracking figure of merit be no greater than 0.1 results in a significant increase in Q , but reduces the polarimeter figure of merit by a factor of four. Restricting the Compton-scattering angle ψ to a range where the analyzing power is greatest also results in a significant increase in Q , but reduces the figure of merit by more than a factor of two. Since the figure of merit depends on both Q and ε , these results indicate that the gain in polarization sensitivity from these cuts is not sufficient to overcome the loss in efficiency. In an experiment where statistics are the main limiting factor, using the entire data set makes the best use of the available information.

4. Simulations

Simulations can be an invaluable tool when planning an experiment. They can provide a realistic prediction of the quality of the data that one may expect from an experiment, and also serve as a guide to the quantity of data needed to achieve a given statistical uncertainty. In this section, we describe simulation software which can be used to predict the performance of GRETINA as a Compton polarimeter under experimental conditions.

The simulation program UCGretina [30], which is based on the Monte Carlo toolkit Geant4 [31], was used in the present work. The core Geant4 libraries already include the ability to describe the polarization state of an atomic nucleus based on the formalism described by Alder and Winther[19], which will automatically generate the correct angular distribution $W(\theta)$. However, a description of the polarization state of photons emitted from an oriented nucleus had not been implemented within the framework as of the time of this writing. Two updates to UCGretina were therefore necessary: (1) a mechanism to provide the magnetic substate population as an input to the simulations in order to leverage the existing polarization code,

and (2) derive the polarization state of the emitted photons in order to generate the asymmetry in the azimuthal Compton-scattering distribution.

4.1. Updates to UCGretina

Of the two updates to UCGretina which were necessary for this study, deriving the polarization state of the emitted photons is by far the more involved. The existing machinery to describe oriented nuclear states within Geant4 is based upon the concept of the density matrix [19], or alternatively the statistical tensor. However, the polarization state of a photon within Geant4 is described by the Stokes parameters, and so it is necessary to derive them from the statistical tensor. This derivation and the resulting implementation in Geant4 will be the subject of a separate publication.

Providing the magnetic substate populations to Geant4 is relatively simple. The orientation of the initial nuclear state is described by the statistical tensor $\rho_{k\kappa}(I_i)$. Because of the axial symmetry about the beam axis, $\rho_{k\kappa}(I_i) = 0$ for $\kappa \neq 0$ [32] and we have [33]:

$$\rho_{k0}(I_i) = \frac{\sqrt{2I_i + 1}}{\sqrt{2k + 1}} \sum_{M_i} (-1)^{I_i - M_i} \langle I_i M_i I_i - M_i | k 0 \rangle P(M_i), \quad (11)$$

where the term in brackets is a Clebsch-Gordan coefficient. The extra factor of $\sqrt{2k + 1}$ compared to Ref. [33] is inserted in order to agree with the notation of Ref. [19], on which the implementation of nuclear alignment is based in Geant4.

4.2. Comparison with data

The modified code was benchmarked against the experimental data described in Sect. 3. Simulations were performed for both the β decay of ^{60}Co and for the $^{24}\text{Mg}(p, p')$ reaction. Both the in-beam and source simulations were run for 40 sets of 10,000,000 events each. The magnetic substate populations $P(M = 0) = 0.52$, $P(M = \pm 1) = 0.24$, and $P(M = \pm 2) = 0$ were derived from the a_2 and a_4 coefficients measured in the experiment and used as an input to the in-beam simulations. No particle detectors were used during the experiment, and so the properties of the beam could not be monitored. For the purposes of the simulations, it was assumed that the beam was well-collimated (no angular divergence) and that the beam spot was focused to a circle of 1 mm diameter.

UCGretina does not attempt to reproduce the finite energy resolution or position resolution for the γ -ray interaction points in GREYINA. The simulations were therefore post-processed by a program which takes the simulated interaction-point energies and positions and treats them as the mean of a Gaussian distribution with configurable width. In order to demonstrate that the simulation is performing correctly, in this section the position resolution is fixed at 0 mm, which would correspond to perfect knowledge of the interaction points in the data. The impact of varying the position resolution is explored in Sect. 4.3.

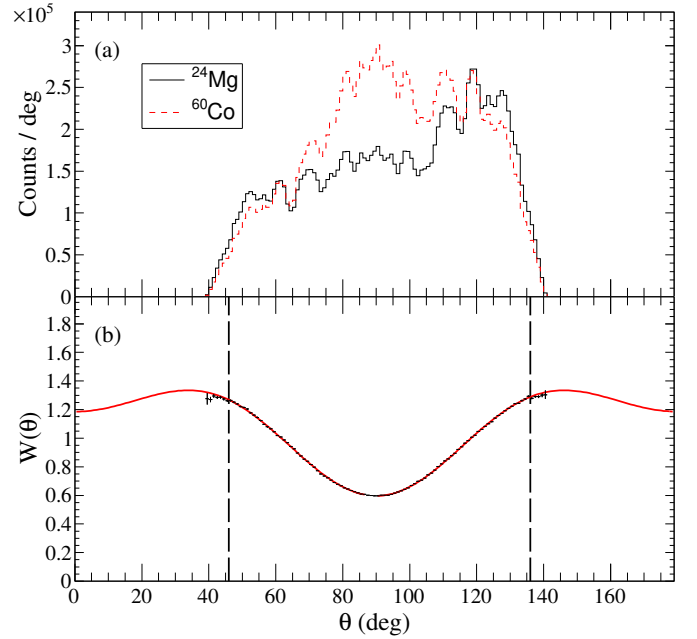


Figure 8: (a) Polar angular distribution of simulated γ rays for the $2_1^+ \rightarrow 0_1^+$ transition in ^{24}Mg (solid line) and the β decay of ^{60}Co (dashed line). (b) The ratio of the ^{24}Mg distribution and ^{60}Co distribution shown in (a). The solid line is the result of a Legendre polynomial fit within the vertical dashed lines, with $a_2 = 0.540(5)$ and $a_4 = -0.354(5)$.

The polar angular distribution generated by the simulations is shown in Fig. 8. As with the experimental data, panel (a) shows the distribution of the emission angles for the in-beam and source simulations (solid and dashed lines, respectively), while panel (b) is the ratio between the two distributions. The solid line in panel (b) is the Legendre series fit, which uses the same range and excludes the same bins as the experimental data in order to provide a direct comparison. The coefficients from the fit are $a_2 = 0.540(5)$ and $a_4 = -0.354(5)$, in agreement with the fit to the experimental data. The degree of polarization derived from these parameters is $P(\theta = 90^\circ) = 0.99(2)$. The agreement with the data demonstrates that the statistical tensor is being calculated correctly from the magnetic substate populations.

The azimuthal scattering-angle distribution for the simulated data (with $80^\circ \leq \theta \leq 100^\circ$) is shown in Fig. 9. As with the experimental data, panel (a) shows the simulated in-beam data and simulated source data (solid and dashed lines, respectively), while panel (b) shows their ratio. The ratio is fit with Eq. 7, resulting in an asymmetry $A_0 = 0.196(1)$. This is roughly double the asymmetry measured for the experimental data, a point which is discussed in Sect. 4.3.

Since the asymmetry is so much larger in the simulation than in the data, it can be anticipated that the polarization sensitivity and figure of merit will be similarly enhanced. Figure 10(b) shows $Q(\theta)$ for the simulated data, with the polarization derived from the a_2 and a_4 coefficients.

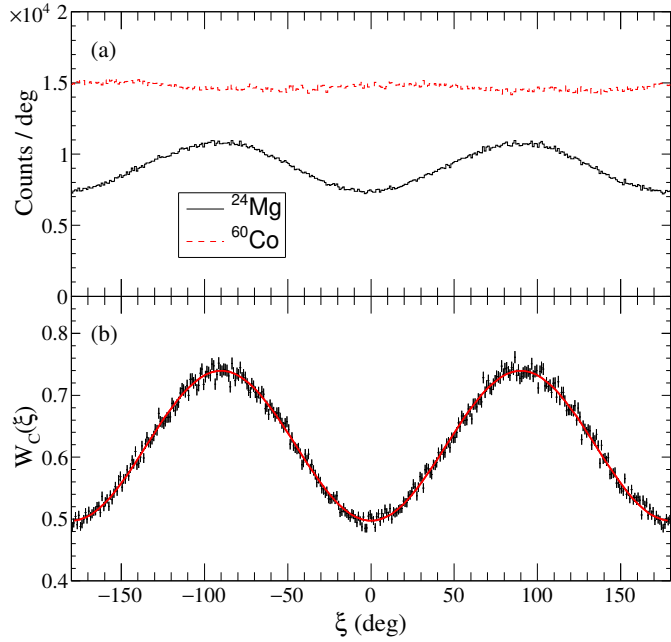


Figure 9: (a) Azimuthal angular distribution of simulated Compton-scattered photons for the $2_1^+ \rightarrow 0_1^+$ transition in ^{24}Mg (solid line) and β^- decay of ^{60}Co (dashed line). As with the data, the first interaction point is restricted to lie in the range $80^\circ \leq \theta \leq 100^\circ$. (b) The ratio of the ^{24}Mg distribution and ^{60}Co distribution shown in (a). The solid line is a fit to the data with Eq. 7, with an asymmetry $A_0 = 0.196(2)$.

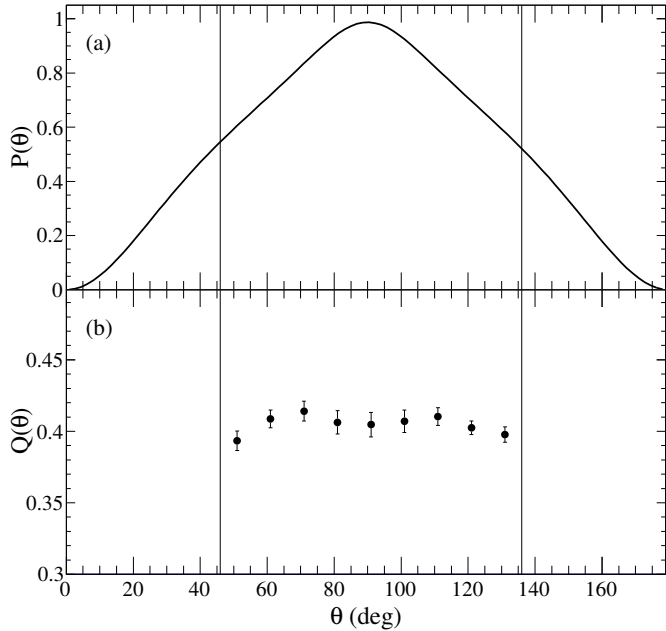


Figure 10: (a) The polarization as a function of the angle θ for the simulations, determined from the a_2 and a_4 coefficients. (b) $Q(\theta)$ for the simulations. As expected, within the uncertainty, Q is not correlated with the γ -ray emission angle.

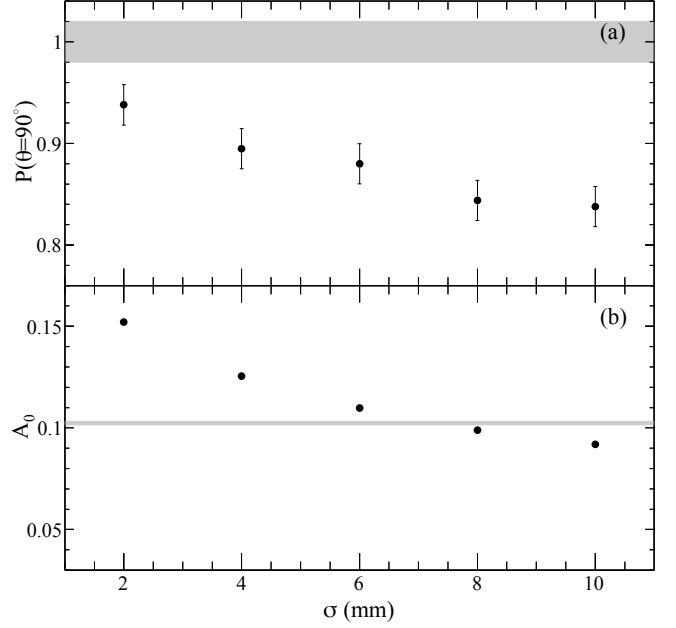


Figure 11: The impact of the position resolution used in the post-processing program applied to the output from UCGretina. The horizontal gray bars indicate the range of $P(\theta = 90^\circ)$ and A_0 values which fall within 1σ of the experimental values. (a) The apparent linear polarization of the photon at 90° as a function of the position smearing. (b) The measured asymmetry in the ξ distribution as a function of the position smearing.

483 coefficients in Fig. 10(a). As expected, it scales with the asymmetry and has a value of roughly 0.4, independent of the
 484 emission angle. Taken over the entire angular range covered in this GRETINA configuration, $Q = 0.392(4)$ for
 485 the simulations. The simulated efficiency can be directly computed based on the number of simulated events and
 486 the number of observed Compton-scattering events after tracking has been performed, which comes out to 4.48(2)%
 487 and can be compared to 5.3(1)% determined for the experimental data. The resulting figure of merit is $6.9(1) \times 10^{-3}$,
 488 clearly much larger than the corresponding value from the experiment.
 489
 490
 491
 492
 493
 494

4.3. Impact of position resolution

495 The enhancement of the asymmetry in the simulations relative to the data is likely due to the perfect position
 496 information available from UCGretina, which clearly does not reflect the experimental reality. To address this issue,
 497 the aforementioned post-processing program was used to add a random offset to the recorded interaction positions.
 498 The offset was sampled from a three-dimensional Gaussian distribution of a set width. This width was determined
 499 according to the relation $\sigma = a + b/\sqrt{e}$ as discussed in Ref [26], where a and b are parameters and e is the energy
 500 deposited at the interaction point. One parameter was fixed by using the 1.2 mm position resolution inferred at
 501 1779 keV in Ref. [25], while the other was fixed by varying the position resolution at 100 keV. The resulting files were
 502
 503
 504
 505

510 analyzed under the same conditions used in Sect. 4.2, and
 511 the resulting polarization at 90° and Compton-scattering
 512 asymmetry are shown Fig. 11. The horizontal axis indic-
 513 ates the resolution used at 100 keV. The horizontal
 514 bars show the 1σ uncertainty in the photon polarization
 515 and asymmetry derived from the experimental data. The
 516 results suggest that the asymmetry in the ξ distribution
 517 matches the data with a position resolution of about 7 mm
 518 at 100 keV, which corresponds to approximately the size
 519 of a segment. However, the deduced polarization at 90°
 520 drops to about 0.85. This should not be interpreted as evi-
 521 dence that GRETA has a 7 mm position resolution at
 522 100 keV; rather, this is a choice of simulation parameters
 523 which gives a reasonable approximation to experimental
 524 data.

525 It is surprising that the photon polarization deduced at
 526 90° drops so rapidly with increasing simulated position
 527 resolution, which is at variance with the results derived from
 528 the experimental data. However, we have observed that
 529 different behavior is obtained if the untracked simulations
 530 are analyzed. In this case, the first interaction point within
 531 a crystal is assumed to have the highest energy, while the
 532 second is assumed to have the next-highest energy. Under
 533 these conditions, $P(\theta = 90^\circ)$ becomes almost independent
 534 of the simulated position resolution, as expected, while
 535 the asymmetry dependence changes only slightly. The results
 536 obtained for the experimental data are similar for the
 537 tracked and untracked data. A possible explanation
 538 for this behavior is that simply smearing the interaction-
 539 point positions, as is done in the post-processing code, is
 540 not a very good approximation to the signal decomposi-
 541 tion process applied to experimental data. As a result, the
 542 tracking algorithm misidentifies the first interaction point
 543 for the simulated data. We are continuing to investigate
 544 ways to ameliorate this issue.

545 Using the energy-dependent position resolution with
 546 $\sigma = 7$ mm at 100 keV, the simulated Q and figure-of-
 547 merit values can be revisited. Repeating the previous
 548 analysis with the appropriate post-processed simulation
 549 results in $Q = 0.207(2)$, very close to what was measured
 550 in the experiment. The efficiency is unchanged by the
 551 post-processing program, and so the figure of merit can be
 552 directly calculated as $F = 1.9(5) \times 10^{-3}$, which is consis-
 553 tent with the experimental result.

554 4.4. Prediction for GRETA

555 With the polarization sensitivity of GRETINA char-
 556 acterized, it is possible to predict the performance of
 557 GRETA. To make this prediction, simulations were per-
 558 formed using the same input parameters as were used
 559 for the simulations of GRETINA, including the same
 560 $^{24}\text{Mg}(p, p')$ reaction with the magnetic substate popu-
 561 lations measured in the experiment, but using the full
 562 GRETA geometry. The energy-dependent position reso-
 563 lution was used in the post-processing, with $\sigma = 7$ mm at
 564 100 keV. The simulations were performed assuming the ex-
 565 istence of γ rays at intervals of 500 keV from 500-2000 keV.

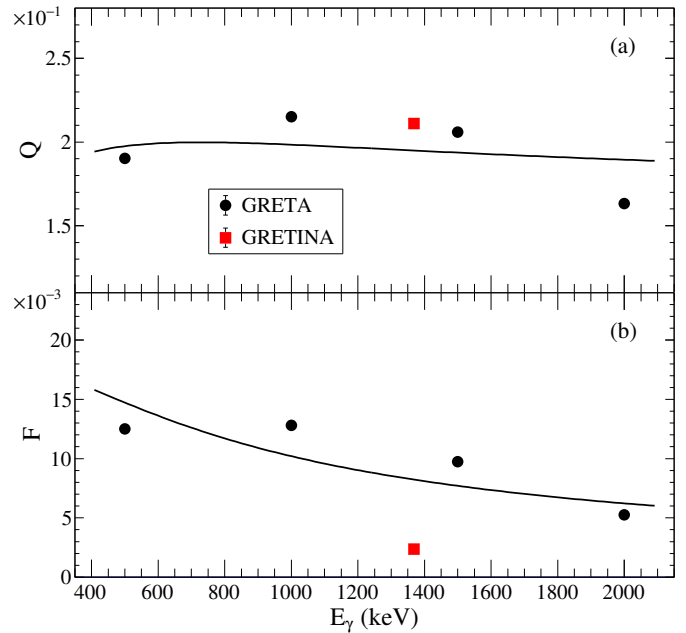


Figure 12: (a) The predicted polarization sensitivity Q for GRETA, based on simulations performed at the energies displayed. (b) The figure of merit F extracted from the simulations for GRETA. The circular points are the simulations of GRETA, while the squares indicate the experimental values measured for GRETINA for comparison. The value of Q deduced for GRETINA at 1368 keV from the experimental data agrees well with the values predicted for GRETA, while the figure of merit is enhanced significantly due to the increased efficiency.

A second set of simulations were run with unpolarized excited states at the same set of energies in order to generate isotropic distributions for normalization. Clearly this does not represent a physical scenario, but it is a convenient means for demonstrating the simulated performance of GRETA.

The results of the GRETA simulations are shown in Fig. 12. The simulated performance of GRETA is given by the circular points, while the squares indicate the values obtained from the experimental data in Sect. 3. Error bars are included in the figure, but in most cases they are smaller than the size of the data points. Panel (a) shows the polarization sensitivity Q as a function of γ -ray energy. It can be seen that the predicted value of Q for GRETA is consistent with the measured value for GRETINA at 1368 keV. This is expected, since the value of Q does not depend on the polar angle. Thus, the additional detectors present in GRETA should not change Q .

The performance of Compton polarimeters is sometimes compared to the characteristics expected of a polarimeter composed of point-like detectors arranged to detect scattering at $\psi = 90^\circ$, which would be the ideal geometry for 0 keV photons if efficiency was not a concern. The polarization sensitivity for such a detector as a function of

γ -ray energy can be expressed [27]

$$Q_p(E_\gamma) = \left(\frac{1}{E_\gamma/511 + 511/(E_\gamma + 511)} \right), \quad (12)$$

where E_γ is in keV. Real polarimeters can be compared to this ideal behavior by applying a scaling factor to Eq. 12 such that [23]

$$Q(E_\gamma) = (P_0 + P_1 E_\gamma) Q_p(E_\gamma). \quad (13)$$

The solid line in Fig. 12(a) is a fit to the simulated polarization sensitivity of GRETA with Eq. 13, with $P_0 = 0.131(6)$ and $P_1 = 3.25(7) \times 10^{-4}$. In principle, GRETA should be a reasonable approximation to a point-like detector, given its ability to localize individual interaction points. The reduction in Q compared to the point-like geometry is likely due to the fact that GRETA is not restricted to detecting scattering at $\psi = 90^\circ$.

The predicted figure of merit for GRETA, shown as a function of energy in Fig. 12(b), is increased drastically compared to the value measured for GRETINA. This can be attributed to the increased efficiency of GRETA relative to GRETINA, as there is five-fold increase in the number of Quad modules (30 compared to six) and the figure of merit scales directly with efficiency. Compared to the polarimeters in Table 1, Fig. 12 suggests that the performance GRETA will be as much as four orders of magnitude better in terms of the figure of merit. The solid line in the figure is the function $F = Q^2 \varepsilon$, where Q is the same as the fit in panel (a) of the figure. In Ref. [25], the singles efficiency of GRETINA with eight Quads is fit and reported as $\varepsilon = 4.532(E_\gamma + 100)^{-0.621}$. Using this function for the efficiency, with a free parameter acting as an overall scaling factor, the fit to the simulated data suggests that the efficiency is equivalent to 35 individual Quad modules. Since the efficiency in Ref. [25] is the singles efficiency, the $\approx 15\%$ gain can reasonably be attributed to events which are recovered through tracking.

5. Conclusion

In this work, we have performed an experiment using the $^{24}\text{Mg}(p, p')$ reaction at 2.45 MeV proton energy in order to characterize the polarization sensitivity of GRETINA in a six-Quad configuration. We have demonstrated that GRETINA can serve as a good polarimeter in terms of the polarization sensitivity Q , and that its performance greatly surpasses previous polarimeters in terms of its figure of merit due to its superior detection efficiency. We have also added the capability to simulate the emission of polarized photons to the UCGretina simulation package, in order to provide a tool for experimenters to judge the quality of the data they can expect from experiments. Finally, we have used UCGretina to predict the performance of GRETA as a polarimeter, and find that its figure of merit should surpass that of GRETINA by a significant margin.

Acknowledgments

This material is based upon work supported by the U.S. Department of Energy, Office of Science, Office of Nuclear Physics under Contract Nos. DE-AC02-05CH11231 (LBNL), DE-AC02-06CH11357 (ANL), and DE-AC02-98CH10946 (BNL), and Grants No. DE-FG02-97ER41041 (UNC) and DE-FG02-97ER41033 (TUNL). This work was also supported in part by the U.S. National Science Foundation grant No. 1401574. GRETINA was funded by the U.S. DOE, Office of Science, Office of Nuclear Physics and operated by the ANL contract number above and by Contract No. DE-AC02-05CH11231 (LBNL). This research used resources of the ATLAS facility at ANL, which is a DOE Office of Science User Facility.

References

- [1] F. Metzger, M. Deutsch, *A study of the polarization-direction correlation of successive gamma-ray quanta*, Phys. Rev. 78 (1950) 551–558. doi:10.1103/PhysRev.78.551. URL <https://link.aps.org/doi/10.1103/PhysRev.78.551>
- [2] C. Broude, O. Häusser, H. Malm, J. Sharpey-Schafer, T. Alexander, *A ge(li) two crystal compton spectrometer*, Nuclear Instruments and Methods 69 (1) (1969) 29–34. doi:https://doi.org/10.1016/0029-554X(69)90568-0. URL <https://www.sciencedirect.com/science/article/pii/0029554X69905680>
- [3] A. E. Litherland, G. T. Ewan, S. T. Lam, *Use of single planar ge(li) detectors as gamma-ray polarimeters*, Can. J. Phys. 48 (19) (1970) 2320–2330. arXiv:https://doi.org/10.1139/p70-289, doi:https://doi.org/10.1139/p70-289. URL <https://doi.org/10.1139/p70-289>
- [4] P. A. Butler, P. E. Carr, L. L. Gadeken, A. N. James, P. J. Nolan, J. F. Sharpey-Schafer, P. J. Twin, D. A. Viggars, *Construction and use of a three ge(li) compton polarimeter*, Nucl. Instrum. Methods 108 (3) (1973) 497–502. doi:https://doi.org/10.1016/0029-554X(73)90530-2. URL <https://www.sciencedirect.com/science/article/pii/0029554X73905302>
- [5] A. Filevich, M. Behar, G. García Bermúdez, *Gamma-gamma polarized directional correlations set-up using a planar ge(li) detector as the polarimeter*, Nuclear Instruments and Methods 141 (3) (1977) 521–524. doi:https://doi.org/10.1016/0029-554X(77)90648-6. URL <https://www.sciencedirect.com/science/article/pii/0029554X77906486>
- [6] R. Bass, J. Idzko, H. Pelz, K. Stelzer, Th. Weber, R. Weniger, *Symmetrical four-crystal compton polarimeter for gamma rays: Design and application*, Nucl. Instrum. Methods 163 (2) (1979) 377. doi:https://doi.org/10.1016/0029-554X(79)90122-8.
- [7] B. Schlitt, U. Maier, H. Friedrichs, S. Albers, I. Bauske, P. von Brentano, R. D. Heil, R.-D. Herzberg, U. Kneissl, J. Margraf, H. H. Pitz, C. Wesselborg, A. Zilges, *A sectored ge-compton polarimeter for parity assignments in photon scattering experiments*, Nucl. Instrum. Methods Phys. Res. A 337 (2) (1994) 416–426. doi:https://doi.org/10.1016/0168-9002(94)91111-8.
- [8] G. Duchêne, F. Beck, P. Twin, G. de France, D. Curien, L. Han, C. Beausang, M. Bentley, P. Nolan, J. Simpson, *The clover: a new generation of composite ge detectors*, Nuclear Instruments and Methods in Physics Research Section A: Accelerators, Spectrometers, Detectors and Associated Equipment 432 (1) (1999) 90–110. doi:https://doi.org/10.1016/S0168-9002(99)00277-6. URL <https://www.sciencedirect.com/science/article/pii/S0168900299002776>

- [9] D. Miller, A. Chester, V. Moeller, K. Starosta, C. Vaman, D. Weisshaar, [Linear polarization sensitivity of sega detectors](#), Nuclear Instruments and Methods in Physics Research Section A: Accelerators, Spectrometers, Detectors and Associated Equipment 581 (3) (2007) 713–718. doi:<https://doi.org/10.1016/j.nima.2007.07.141>. URL <https://www.sciencedirect.com/science/article/pii/S0168900207016464>
- [10] A. Khaplanov, S. Tashenov, B. Cederwall, G. Jaworski, [A \$\gamma\$ -ray polarimeter based on a single segmented planar hpge detector](#), Nuclear Instruments and Methods in Physics Research Section A: Accelerators, Spectrometers, Detectors and Associated Equipment 593 (3) (2008) 459–465. doi:<https://doi.org/10.1016/j.nima.2008.05.063>. URL <https://www.sciencedirect.com/science/article/pii/S0168900208007948>
- [11] I. Y. Lee, M. A. Deleplanque, K. Vetter, Developments in large gamma-ray detector arrays, Rep. Prog. Phys. 66 (7) (2003) 1095–1144. doi:[10.1088/0034-4885/66/7/201](https://doi.org/10.1088/0034-4885/66/7/201).
- [12] S. Paschalis, I. Y. Lee, A. O. Macchiavelli, C. M. Campbell, M. Cromaz, S. Gros, J. Pavan, J. Qian, R. M. Clark, H. L. Crawford, D. Doering, P. Fallon, C. Lionberger, T. Loew, M. Petri, T. Stezelberger, S. Zimmermann, D. C. Radford, K. Lagergren, D. Weisshaar, R. Winkler, T. Glasmacher, J. T. Anderson, C. W. Beausang, The performance of the gamma-ray energy tracking in-beam nuclear array gretina, Nucl. Instrum. Methods Phys. Res. A 709 (2013) 44. doi:<https://doi.org/10.1016/j.nima.2013.01.009>.
- [13] GRETA Conceptual Design Report, <http://greta.lbl.gov/documents/ConceptualDesignReport-071717.pdf>, accessed: 2021-10-31.
- [14] S. Akkoyun, A. Algora, B. Alikhani, F. Ameil, G. de Angelis, L. Arnold, A. Astier, A. Ataç, Y. Aubert, C. Aufranc, A. Austin, S. Aydin, F. Azaiez, S. Badoer, D. L. Balabanski, D. Barrientos, G. Baulieu, R. Baumann, D. Bazzacco, F. A. Beck, T. Beck, P. Bednarczyk, M. Bellato, M. A. Bentley, G. Benzoni, R. Berthier, L. Berti, R. Beunard, G. Lo Bianco, B. Birkenbach, P. G. Bizzeti, A. M. Bizzeti-Sona, F. Le Blanc, J. M. Blasco, N. Blasi, D. Bloor, C. Boiano, M. Borsato, D. Bortolato, A. J. Boston, H. C. Boston, P. Bourgault, P. Boutchikov, A. Bouty, A. Bracco, S. Brambilla, I. P. Brawn, A. Bronchi, S. Broussard, B. Bruyneel, D. Bucurescu, I. Burrows, A. Bürger, S. Cabaret, B. Cahan, E. Calore, F. Camera, A. Capsoni, F. Carrió, G. Casati, M. Castoldi, B. Cederwall, J.-L. Cercus, V. Chambert, M. El Chambit, R. Chapman, L. Charles, J. Chavas, E. Clément, P. Cocconi, S. Coelli, P. J. Coleman-Smith, A. Colombo, S. Colosimo, C. Commeaux, D. Conventi, R. J. Cooper, A. Corsi, A. Cortesi, L. Costa, F. C. L. Crespi, J. R. Cresswell, D. M. Cullen, D. Curien, A. Czermak, D. Delbourg, R. Depalo, T. Descombes, P. Désesquelles, P. Detistov, C. Diarra, F. Didierjean, M. R. Dimmock, Q. T. Doan, C. Domingo-Pardo, M. Doncel, F. Dorangeville, N. Dosme, Y. Drouen, G. Duchêne, B. Dulny, J. Eberth, P. Edelbruck, J. Egea, T. Engert, M. N. Erduran, S. Ertürk, C. Fanin, S. Fantinel, E. Farnea, T. Faul, M. Filliger, F. Filmer, Ch. Finck, G. de France, A. Gadea, W. Gast, A. Geraci, J. Gerl, R. Gernhäuser, A. Giannatiempo, A. Giaz, L. Gibelin, A. Givechev, N. Goel, V. González, A. Gottardo, X. Grave, J. Grebosz, R. Griffiths, A. N. Grint, P. Gros, L. Guevara, M. Gulmini, A. Görgen, H. T. M. Ha, T. Habermann, L. J. Harkness, H. Harroch, K. Hauschild, C. He, A. Hernández-Prieto, B. Hervieu, H. Hess, T. Hüyük, E. Ince, R. Isocrate, G. Jaworski, A. Johnson, J. Jolie, P. Jones, B. Jonson, P. Joshi, D. S. Judson, A. Jungclauss, M. Kaci, N. Karkour, M. Karolak, A. Kaşkaş, M. Kebiriri, R. S. Kempley, A. Khaplanov, S. Klupp, M. Kogimtzis, I. Kojouharov, A. Korichi, W. Korten, Th. Kröll, R. Krücken, N. Kurz, B. Y. Ky, M. Labiche, X. Lafay, L. Lavergne, I. H. Lazarus, S. Leboutelier, F. Lefebvre, E. Legay, L. Legeard, F. Lelli, S. M. Lenzi, S. Leoni, A. Lermite, D. Lersch, J. Leske, S. C. Letts, S. Lhenoret, R. M. Lieder, D. Linget, J. Ljungvall, A. Lopez-Martens, A. Lotodé, S. Lunardi, A. Maj, J. van der Marel, Y. Mariette, N. Marginean, R. Marginean, G. Maron, A. R. Mather, W. Meczyński, V. Mendéz, P. Medina, B. Melon, R. Menegazzo, D. Mengoni, E. Merchan, L. Mihailescu, C. Michelagnoli, J. Mierzejewski, L. Milechina, B. Million, K. Mitev, P. Molini, D. Montanari, S. Moon, F. Morbiducci, R. Moro, P. S. Morrall, O. Möller, A. Nannini, D. R. Napoli, L. Nelson, M. Nespolo, V. L. Ngo, M. Nicoletto, R. Nicolini, Y. Le Noa, P. J. Nolan, M. Norman, J. Nyberg, A. Obertelli, A. Olariu, R. Orlandi, D. C. Oxley, C. Özben, M. Ozille, C. Oziol, E. Pachoud, M. Palacz, J. Palin, J. Panchin, C. Parisel, P. Pariset, G. Pascovici, R. Peghin, L. Pellegrini, A. Perego, S. Perrier, M. Petcu, P. Petkov, C. Petrache, E. Pierre, N. Pietralla, S. Pietri, M. Pignanelli, I. Piqueras, Z. Podolyak, P. Le Pouhalec, J. Pouthas, D. Pugnère, V. F. E. Pucknell, A. Pullia, B. Quintana, R. Raine, G. Rainovski, L. Ramina, G. Rampazzo, G. La Rana, M. Rebeschini, F. Recchia, N. Redon, M. Reese, P. Reiter, P. H. Regan, S. Riboldi, M. Richer, M. Rigato, S. Rigby, G. Ripamonti, A. P. Robinson, J. Robin, J. Roccaz, J.-A. Ropert, B. Rossé, C. Rossi Alvarez, D. Rosso, B. Rubio, D. Rudolph, F. Saillant, E. Şahin, F. Salomon, M.-D. Salsac, J. Salt, G. Salvato, J. Sampson, E. Sanchez, C. Santos, H. Schaffner, M. Schlarb, D. P. Scraggs, D. Seddon, M. Şenyiçit, M.-H. Sigward, G. Simpson, J. Simpson, M. Slee, J. F. Smith, P. Sona, B. Sowicki, P. Spolaore, C. Stahl, T. Stanios, E. Stefanova, O. Stéżowski, J. Strachan, G. Suliman, P.-A. Söderström, J. L. Tain, S. Tanguy, S. Tashenov, Ch. Theisen, J. Thornhill, F. Tomasi, N. Toniolo, R. Touzery, B. Travers, A. Triossi, M. Tripon, K. M. M. Tun-Lanoë, M. Turcato, C. Unsworth, C. A. Ur, J. J. Valiente-Dobon, V. Vandone, E. Vardaci, R. Venturelli, F. Veronese, Ch. Veysié, E. Viscione, R. Wadsworth, P. M. Walker, N. Warr, C. Weber, D. Weisshaar, D. Wells, O. Wieland, A. Wiens, G. Wittwer, H. J. Wollersheim, F. Zocca, N. V. Zamfir, M. Ziebliński, A. Zucchiatti, [Agata—advanced gamma tracking array](#), Nucl. Instrum. Methods Phys. Res. A 668 (2012) 26–58. doi:<https://doi.org/10.1016/j.nima.2011.11.081>. URL <https://www.sciencedirect.com/science/article/pii/S0168900211021516>
- [15] P. G. Bizzeti, P. Sona, C. Michelagnoli, B. Melon, D. Bazzacco, E. Farnea, A. M. Bizzeti-Sona, G. de Angelis, A. Gadea, A. Gottardo, S. Lunardi, R. Menegazzo, D. Mengoni, A. Nannini, D. R. Napoli, A. Perego, F. Recchia, E. Şahin, J. J. Valiente-Dobón, C. A. Ur, Analyzing power of agata triple clusters for gamma-ray linear polarization, Eur. Phys. J. A 51 (2015) 49. doi:<https://doi.org/10.1140/epja/i2015-15049-4>.
- [16] B. Alikhani, A. Givechev, A. Heinz, P. R. John, J. Leske, M. Lettmann, O. Möller, N. Pietralla, C. Röder, [Compton polarimetry with a 36-fold segmented hpge-detector of the agata-type](#), Nucl. Instrum. Methods Phys. Res. A 675 (2012) 144–154. doi:<https://doi.org/10.1016/j.nima.2012.02.016>. URL <https://www.sciencedirect.com/science/article/pii/S016890021200174X>
- [17] M. D. Jones, A. O. Macchiavelli, M. Wiedeking, L. A. Bernstein, H. L. Crawford, C. M. Campbell, R. M. Clark, M. Cromaz, P. Fallon, I. Y. Lee, M. Salathe, A. Wiens, A. D. Ayangeakaa, D. L. Bleuel, S. Bottoni, M. P. Carpenter, H. M. Davids, J. Elson, A. Görgen, M. Guttormsen, R. V. F. Janssens, J. E. Kinnison, L. Kirsch, A. C. Larsen, T. Lauritsen, W. Reviol, D. G. Sarantites, S. Siem, A. V. Voinov, S. Zhu, [Examination of the low-energy enhancement of the \$\gamma\$ -ray strength function of \$^{56}\text{Fe}\$](#) , Phys. Rev. C 97 (2018) 024327. doi:[10.1103/PhysRevC.97.024327](https://doi.org/10.1103/PhysRevC.97.024327). URL <https://link.aps.org/doi/10.1103/PhysRevC.97.024327>
- [18] L. W. Fagg, S. S. Hanna, [Polarization measurements on nuclear gamma rays](#), Rev. Mod. Phys. 31 (1959) 711–758. doi:[10.1103/RevModPhys.31.711](https://doi.org/10.1103/RevModPhys.31.711). URL <https://link.aps.org/doi/10.1103/RevModPhys.31.711>
- [19] K. Alder, A. Winther, Electromagnetic Excitation, North-Holland, 1975.
- [20] A. R. Poletti, E. K. Warburton, [Study of the low-lying levels of](#)

- f^{18} by means of the $o^{16}(he^3, p\gamma)f^{18}$ reaction, *Phys. Rev.* 137 (1965) B595–B619. doi:<https://doi.org/10.1103/PhysRev.137.B595>.
URL <https://link.aps.org/doi/10.1103/PhysRev.137.B595>
- [21] O. Klein, Y. Nishina, Über die streuung von strahlung durch freie elektronen nach der neuen relativistischen quantendynamik von dirac, *Z. Phys.* 52 (1929) 853. doi:<https://doi.org/10.1007/BF01366453>.
- [22] A. von der Werth, F. Becker, J. Eberth, S. Freund, U. Hermkens, T. Mylaeus, S. Skoda, H. G. Thomas, W. Teichert, Two compton polarimeter constructions for modern standard γ -spectroscopy, *Nucl. Instrum. Methods Phys. Res. A* 357 (2) (1995) 458–466. doi:[https://doi.org/10.1016/0168-9002\(95\)00025-9](https://doi.org/10.1016/0168-9002(95)00025-9).
URL <https://www.sciencedirect.com/science/article/pii/S0168900295000259>
- [23] P. M. Jones, L. Wei, F. A. Beck, P. A. Butler, T. Byrski, G. Duchêne, G. de France, F. Hannachi, G. D. Jones, B. Khararaja, Calibration of the new composite clover detector as a compton polarimeter for the eurogam array, *Nucl. Instrum. Methods Phys. Res. A* 362 (2) (1995) 556–560. doi:[https://doi.org/10.1016/0168-9002\(95\)00246-4](https://doi.org/10.1016/0168-9002(95)00246-4).
URL <https://www.sciencedirect.com/science/article/pii/S0168900295002464>
- [24] B. A. Logan, R. T. Jones, A. Ljubičić, A figure of merit for gamma-ray polarimeters, *Nucl. Instrum. Methods* 108 (3) (1973) 603–604. doi:[https://doi.org/10.1016/0029-554X\(73\)90545-4](https://doi.org/10.1016/0029-554X(73)90545-4).
URL <https://www.sciencedirect.com/science/article/pii/S0029554X73905454>
- [25] D. Weisshaar, D. Bazin, P. C. Bender, C. M. Campbell, F. Recchia, V. Bader, T. Baugher, J. Belarge, M. P. Carpenter, H. L. Crawford, M. Cromaz, B. Elman, P. Fallon, A. Forney, A. Gade, J. Harker, N. Kobayashi, C. Langer, T. Lauritsen, I. Y. Lee, A. Lemasson, B. Longfellow, E. Lunderberg, A. O. Macchiavelli, K. Miki, S. Momiyama, S. Noji, D. C. Radford, M. Scott, J. Sethi, S. R. Stroberg, C. Sullivan, R. Titus, A. Wiens, S. Williams, K. Wimmer, S. Zhu, The performance of the γ -ray tracking array gretina for γ -ray spectroscopy with fast beams of rare isotopes, *Nucl. Instrum. Methods Phys. Res. A* 847 (2017) 187–198. doi:<https://doi.org/10.1016/j.nima.2016.12.001>.
URL <https://www.sciencedirect.com/science/article/pii/S0168900216312402>
- [26] P.-A. Söderström, F. Recchia, J. Nyberg, A. Al-Adili, A. Ataç, S. Aydin, D. Bazzacco, P. Bednarczyk, B. Birkenbach, D. Bortolato, A. J. Boston, H. C. Boston, B. Bruyneel, D. Bucurescu, E. Calore, S. Colosimo, F. C. L. Crespi, N. Dosme, J. Eberth, E. Farnea, F. Filmer, A. Gadea, A. Gottardo, X. Grave, J. Grebosz, R. Griffiths, M. Gulmini, T. Habermann, H. Hess, G. Jaworski, P. Jones, P. Joshi, D. S. Judson, R. Kempley, A. Kharplanov, E. Legay, D. Lersch, J. Ljungvall, A. Lopez-Martens, W. Meczynski, D. Mengoni, C. Michelagnoli, P. Molini, D. R. Napoli, R. Orlandi, G. Pascovici, A. Pullia, P. Reiter, E. Sahin, J. F. Smith, J. Strachan, D. Tonev, C. Unsworth, C. A. Ur, J. J. Valiente-Dobón, C. Veyssiere, A. Wiens, Interaction position resolution simulations and in-beam measurements of the agata hpge detectors, *Nucl. Instrum. Methods Phys. Res. A* 638 (1) (2011) 96 – 109. doi:<https://doi.org/10.1016/j.nima.2011.02.089>.
- [27] G. J. Schmid, A. O. Macchiavelli, S. J. Asztalos, R. M. Clark, M. A. Deleplanque, R. M. Diamond, P. Fallon, R. Kruecken, I. Y. Lee, R. W. MacLeod, F. S. Stephens, K. Vetter, Gamma-ray polarization sensitivity of the gammasphere segmented germanium detectors, *Nucl. Instrum. Methods Phys. Res. A* 417 (1) (1998) 95–110. doi:[https://doi.org/10.1016/S0168-9002\(98\)00624-X](https://doi.org/10.1016/S0168-9002(98)00624-X).
URL <https://www.sciencedirect.com/science/article/pii/S016890029800624X>
- [28] R. B. Firestone, Nuclear data sheets for $a = 24$, *Nucl. Data Sheets* 108 (11) (2007) 2319–2392. doi:<https://doi.org/10.1016/j.nds.2007.10.001>.
URL <https://www.sciencedirect.com/science/article/pii/S0090375207000877>
- [29] T. Lauritsen, A. Korichi, S. Zhu, A. N. Wilson, D. Weisshaar, J. Dudouet, A. D. Ayangeakaa, M. P. Carpenter, C. M. Campbell, E. Clément, H. L. Crawford, M. Cromaz, P. Fallon, J. P. Greene, R. V. F. Janssens, T. L. Khoo, N. Lalović, I. Y. Lee, A. O. Macchiavelli, R. M. Perez-Vidal, S. Pietri, D. C. Radford, D. Ralet, L. A. Riley, D. Seweryniak, O. Stezowski, Characterization of a gamma-ray tracking array: A comparison of gretina and gammasphere using a $60Co$ source, *Nucl. Instrum. Methods Phys. Res. A* 836 (2016) 46–56. doi:<https://doi.org/10.1016/j.nima.2016.07.027>.
URL <https://www.sciencedirect.com/science/article/pii/S0168900216307434>
- [30] L. A. Riley, D. Weisshaar, H. L. Crawford, M. L. Agiorgousis, C. M. Campbell, M. Cromaz, P. Fallon, A. Gade, S. D. Gregory, E. B. Haldeman, L. R. Jarvis, E. D. Lawson-John, B. Roberts, B. V. Sadler, C. G. Stine, Ucgretina geant4 simulation of the gretina gamma-ray energy tracking array, *Nucl. Instrum. Methods Phys. Res. A* 1003 (2021) 165305. doi:<https://doi.org/10.1016/j.nima.2021.165305>.
URL <https://www.sciencedirect.com/science/article/pii/S0168900221002898>
- [31] S. Agostinelli, J. Allison, K. Amako, J. Apostolakis, H. Araujo, P. Arce, M. Asai, D. Axen, S. Banerjee, G. Barrand, F. Behner, L. Bellagamba, J. Boudreau, L. Broglia, A. Brunengo, H. Burkhardt, S. Chauvie, J. Chuma, R. Chytráček, G. Cooperman, G. Cosmo, P. Degtyarenko, A. Dell’Acqua, G. Depaola, D. Dietrich, R. Enami, A. Feliciello, C. Ferguson, H. Fesefeldt, G. Folger, F. Foppiano, A. Forti, S. Garelli, S. Giani, R. Giannitrapani, D. Gibin, J. J. Gómez Cadenas, I. González, G. Gracia Abril, G. Greeniaus, W. Greiner, V. Grichine, A. Grossheim, S. Guatelli, P. Gumplinger, R. Hamatsu, K. Hashimoto, H. Hasei, A. Heikkinen, A. Howard, V. Ivanchenko, A. Johnson, F. W. Jones, J. Kallenbach, N. Kanaya, M. Kawabata, Y. Kawabata, M. Kawaguti, S. Kelner, P. Kent, A. Kimura, T. Kodama, R. Kokoulin, M. Kossov, H. Kurashige, E. Lamanna, T. Lampén, V. Lara, V. Lefebvre, F. Lei, M. Liendl, W. Lockman, F. Longo, S. Magni, M. Maire, E. Medernach, K. Minamimoto, P. Mora de Freitas, Y. Morita, K. Murakami, M. Nagamatu, R. Nartallo, P. Nieminen, T. Nishimura, K. Ohtsubo, M. Okamura, S. O’Neale, Y. Oohata, K. Paech, J. Perl, A. Pfeiffer, M. G. Pia, F. Ranjard, A. Rybin, S. Sadilov, E. Di Salvo, G. Santin, T. Sasaki, N. Savvas, Y. Sawada, S. Scherer, S. Sei, V. Sirotenko, D. Smith, N. Starkov, H. Stoecker, J. Sulkimo, M. Takahata, S. Tanaka, E. Tcherniaev, E. Safai Tehrani, M. Tropeano, P. Truscott, H. Uno, L. Urban, P. Urban, M. Verderi, A. Walkden, W. Wander, H. Weber, J. P. Wellisch, T. Wenaus, D. C. Williams, D. Wright, T. Yamada, H. Yoshida, D. Zschesche, Geant4—a simulation toolkit, *Nucl. Instrum. Methods Phys. Res. A* 506 (3) (2003) 250 – 303. doi:[https://doi.org/10.1016/S0168-9002\(03\)01368-8](https://doi.org/10.1016/S0168-9002(03)01368-8).
URL <http://www.sciencedirect.com/science/article/pii/S0168900203013688>
- [32] V. V. Balashov, A. N. Grum-Grzhimailo, N. M. Kabachnik, Polarization and Correlation Phenomena in Atomic Collisions, Springer Science+Business Media, 2000.
- [33] T. Yamazaki, Tables of coefficients for angular distribution of gamma rays from aligned nuclei, *Nucl. Data Sheets* 3 (1) (1967) 1–23. doi:[https://doi.org/10.1016/S0550-306X\(67\)80002-8](https://doi.org/10.1016/S0550-306X(67)80002-8).
URL <https://www.sciencedirect.com/science/article/pii/S0550306X67800028>